Regen. Eng. Transl. Med. (2015) 1:32–41
DOI 10.1007/s40883-015-0004-1

Fabrication and Characterization of Three-Dimensional Electrospun Scaffolds for Bone Tissue Engineering

Tea Andric[1] · Brittany L. Taylor[2] · Abby R. Whittington[3,4,5] · Joseph W. Freeman[2]

Received: 5 June 2015 / Accepted: 29 October 2015 / Published online: 18 November 2015

Abstract

There are 600,000 bone-grafting procedures performed annually as a result of significant skeletal loss and bone deficiencies. This is an increasing worldwide medical issue as the average life expectancy increases 2–3 % annually. The current standards for bone treatment are autografts and allografts; both of which have drawbacks. Therefore, there is a need for alternative bone graft substitutes such as tissue-engineered grafts. Tissue engineering has emerged as a promising option for bone treatments by using biological or synthetic scaffolds to promote tissue regeneration. The advantages of this treatment include abundant supply and customizable features. The majority of scaffold fabrication techniques used in research focuses on mimicking the porous trabecular bone structure. A major characteristic of optimal scaffold integration and viability is vascularization, which is housed within the osteon canal of the cortical bone. Namely, there is a lack of tissue-engineered scaffolds for bone regeneration that mimic both trabecular and cortical bone structures. In this study, we combined two previously fabricated structures, sintered electrospun sheets and individual osteon-like scaffolds, to create scaffolds that mimic dual structural organization of the native bone with cortical and trabecular regions. Scaffolds were successfully mineralized in 10× simulated body fluid (SBF) up to 48 h with enhanced mineral distribution throughout the scaffolds. Mineralization for 24 h significantly increased mechanical properties of the scaffolds. In vitro studies performed over 28 days with mouse-pre-osteoblastic cells, MC3T3-E1s, proved that the mineralized scaffolds promoted cellular attachment, proliferation, and early stages of osteoblastic differentiation in comparison to the non-mineralized scaffolds. The implications of this study lead to the advancement of tissue-engineered mineralized trabecular and cortical bone scaffolds.

Lay Summary

The use of tissue-engineered scaffolds to harness a patients' own bone regenerative properties following traumatic bone loss has emerged as an alternative to current bone-grafting procedures. In this manuscript, the development and characterization process of a synthetic scaffold which mimics both the porous trabecular bone structure and dense cortical bone structure is discussed. Qualitative analysis confirmed the biomimetic porous structure necessary for nutrient transport and cellular infiltration and the cortical canal structure to house vascularization. Various mineralization techniques were investigated to determine the optimal mechanical properties. The scaffold also exhibited the ability to promote osteoblastic cellular attachment and proliferation. The mineral content deposited onto the scaffold led to an increase in osteoblastic behavior of the attached cells; suggesting early stages of osteogenesis. The results of this manuscript indicate the potential of utilizing a tissue-engineering scaffold as a promising treatment for bone tissue regeneration applications.

✉ Joseph W. Freeman
joseph.freeman@rutgers.edu

[1] University of Virginia Health System, University of Virginia, Charlottesville, VA, USA

[2] Department of Biomedical Engineering, Rutgers University, Piscataway, NJ, USA

[3] School of Biomedical Engineering and Sciences, Virginia Tech-Wake Forest University, Blacksburg, VA, USA

[4] Material Science and Engineering, Virginia Tech, Blacksburg, VA, USA

[5] Department of Chemical Engineering, Virginia Tech, Blacksburg, VA, USA

Keywords Tissue engineering · Bone · Electrospinning · Scaffold mineralizaiton · Mouse pre-osteoblasts

Introduction

Skeletal loss and bone deficiencies are major worldwide orthopedic concerns resulting in approximately 600,000 bone-grafting procedures performed annually. The annual bone grafting market is projected to reach $3.5 billion by 2023 due to the increasing average life expectancy [1–3] . Autograft is the current standard in orthopedic reconstructive surgeries with a high success rate, but disadvantages associated with this procedure include limited supply, donor site morbidity, and increased costs. The use of allografts as an alternative method eliminates the potential drawbacks seen with autografts, but their associated limitations include risk of disease transmission and high mechanical and structural failure rates in vivo due to the harsh decellularization and sterilization techniques. These disadvantages lead to the need for an alternative grafting option for bone reconstruction and regeneration.

The bone is a composite tissue organized into trabecular (or cancellous) and cortical (or compact) bone structures. The cortical bone is usually located on the outer parameter of a bone structure, highly organized, compact, and dense. The subunits of the cortical bone are tightly packed structures called osteons. Osteons, ranging from 100 to 300 μm in diameter, are oriented parallel along the long axis of the bone. Vasculature and nerves are housed within the central Haversian canal [4–6]. The cortical bone exhibits high tensile (107–140 MPa) and compressive (167–215 MPa) mechanical properties and a Young's modulus of 10–20 GPa due to its highly organized concentric structure of mineralized collagen fibers [7]. The trabecular bone is the highly porous type of bone that is located in the center of the cortical bone structures.The trabecular bone has a wider range of and lower mechanical properties than the cortical bone and due to its is 90 % porous profile [5, 7, 8]. The interconnected network exhibited in the trabecular bone is essential for nutrient support and cellular infiltration. The trabecular bone has compressive strength in the range of 3–9 MPa and Young's modulus of 0.01–0.9 GPa [7].

A large number of scaffold fabrication techniques are being investigated for applications in tissue engineering of the bone [9–14]. Average pore size, porosity, pore interconnectivity, and mechanical properties of the scaffold will vary when comparing different techniques. Porosity and interconnectivity play an important role in tissue regeneration, as it is necessary for migration and proliferation of the cells and tissue formation within the scaffolds. Higher porosities and larger pore sizes enhance bone ingrowth and osseointegration. The optimal pore sizes for scaffolds have been reported to range from 100 to 300 μm [9, 14–17]. While macroporosity is important for tissue integration, microporosity and surface roughness also play a role in cellular attachment, proliferation, and differentiation [9, 14–17]. Some of the techniques currently investigated for scaffold fabrications include thermally induced phase separation (TIPS), solvent casting/particulate leaching, heat sintering microspheres, and electrospinning.

Thermally induced phase separation (TIPS) is a technique used to create highly porous 3-D scaffolds by dissolving polymer in a solvent at a higher temperature and then inducing liquid-liquid or liquid-solid phase separation by lowering the temperature. Porosity, pore size, and pore orientation are controlled by controlling polymer concentration and temperature gradient [10, 18, 19]. Solvent casting/particulate leaching is a scaffold fabrication technique where water-soluble particles or paraffin are used as space holders for future pore networks, while polymer solution is cast around them. After the solvent is evaporated and polymer set, the porogens are leached out leaving a pore network behind. Porosity and pore size depend on the porogen size [19–21]. While the use of porogens provides the control of pore size and porosity, interconnectivity of the pores can still be a problem [10, 11, 20–23]. Heat sintering is a technique where the polymer microspheres are heated above glass transition (Tg) of polymer and held for certain period of time and then cooled down to room temperature. During the heating process, the sintering occurs due to the intertwining of polymer chains between adjacent microspheres, forming bonds. By controlling the size of the microspheres and heat sintering time, the pore size and porosity can be controlled [24–26]. Each processing technique has advantages and disadvantages for applications in bone tissue engineering, but all the techniques seek to create scaffolds that have uniform structure and porosity throughout the scaffolds, unlike the natural dual organization in natural bone. Very few techniques and approaches have focused on creating scaffolds that mimic dual structural organization found in natural bone tissue [27, 28].

Synthetic polymers offer unique benefits for fabrication techniques, as they are produced under controlled conditions giving them predictable and reproducible mechanical and degradation properties [11]. While many biodegradable synthetic polymers are available, poly(α-hydroxy acid)s, a subgroup of polyesters, are most commonly used due to their ease of processing, biocompatibility, wide range of degradation rates, good mechanical properties, and are also FDA approved [10–12, 29, 30]. The primary materials used to create the base of the scaffold are two polyesters poly (α-hydroxy acid) polyesters, poly-l-lactide (PLLA), and poly-d-lactide (PDLA). PLLA and PDLA were selected based on their favorable materials properties, as shown in Table 1. The monomers of PLLA and PDLA have a central carbon atom with terminal carboxyl group (-COOH) and a terminal methyl group (CH_3). PLLA is a semi-crystalline polymer with a higher tensile

Table 1 Material properties of PLLA and PDLA [31]

	Degradation rate	Tensile strength	Tensile modulus	Glass transition temperature
PLLA	>24 months	60–70 MPa	3GPa	60–65°C
PDLA	12–15 months	40–50 MPa	2GPa	44–55°C

strength and a slower degradation than PDLA, which is less crystalline. Both polymers degrade via hydrolytic degradation [32, 33]. PDLA, which has a low glass transition temperature, is used as the bonding agent to hold the scaffold layers together when sintered at its glass transition temperature.

In this study, we will focus on creating fabricated scaffolds that mimic both architectures of the native bone by replicating the highly dense cortical structure and porosity of the trabecular bone. To do this, we will utilize the electrospinning technique to create scaffolds that mimic the nanofibrous architecture of natural extracellular matrix. Extracellular matrix is a network of fibrous structure involved in cell adhesion, cell-to-cell communication, and differentiation. The woven fibrous scaffold will serve as a matrix for the attachment, proliferation, and migration of cells involved in bone regeneration. Electrospun scaffolds are characterized by high surface area, high porosities, and interconnected pore networks [34, 35]. Our group has employed a heat sintering technique to create three-dimensional electrospun scaffolds, which allows us to investigate and tune the scaffold's compressive mechanical properties. It also allows us to combine different electrospun structures to create unique and more tailored scaffold architectures. We combined two previously fabricated structures, sintered electrospun sheets, and individual osteon-like scaffolds [36], to create scaffolds that mimic dual structural organization of the natural bone with cortical and trabecular regions. Scaffolds were mineralized by incubation in 10× simulated body fluid (SBF) and characterized to determine mechanical properties, mineral deposition and distribution, and cellular activity on the scaffolds.

Materials and Methods

Electrospinning Cortical and Trabecular Scaffolds

Poly (L-lactide) (PLLA) (inherent viscosity =2.0 dl/g, Mw= 152,000) was purchased from Sigma-Aldrich (St. Louis, MO, USA). Poly (D, L-lactide) (PDLA) (inherent viscosity 0.6–0.8 dL/g) was purchased from SurModics Pharmaceuticals (Birmingham, AL, USA). Dichloromethane (DCM), tetrahydrofuran (THF), and dimethylformaldehyde (DMF) were purchased from Fisher Scientific (Pittsburgh, PA, USA). Gelatin, type A, from the porcine skin was purchased from Sigma-Aldrich (St. Louis, MO, USA). NaCl, KCl, CaCl $2H_20$, $MgCl_2$ $6H_20$, $NaHCO_3$, and NaH_2PO_4 were purchased from Fisher Scientific (Pittsburgh, PA, USA).

The electrospinning solutions were prepared by dissolving PLLA to 7 % w/v in 75 % DCM and 25 % DMF, and dissolving PDLA to 22 % w/v in 75 % THF and 25% DMF. The PLLA/gelatin mixture was made by dissolving gelatin in 1-ml deionized (dI) water and adding it to the 7 % PLLA solution. The amount of gelatin in solution is equal to 10 %, w/w of the amount of PLLA in the solution. The solutions were vortexed for 1 h to homogenize the solution before electrospinning. Polymer solutions were made in 16 ml batches, and to make overall volume of gelatin/PLLA and PLLA solutions equal, 1 ml of DCM is replaced with 1 ml of gelatin.

First, the PDLA solution was loaded into a 5-ml plastic syringe with an 18-gage needle and extruded at a rate of 5 mL/h. PDLA was electrospun on a rotating (~2000 RPM) 5-cm diameter mandrel for a total volume of 1 ml, at a working distance of 15 cm with voltages of +12 kV and −5 kV applied. The gelatin/PLLA was then electrospun directly onto the PDLA layer with a working distance of 5 cm. The voltages applied were +18 kV and −7 kV. An additional layer of 1-ml PDLA was electrospun on top of gelatin/PLLA layer. Electrospinning conditions were maintained at 37°C and between 10 and 20 % ambient relative humidity.

Poly (ethylene oxide) was dissolved in 10 % of 100 % ethanol and 90 % of dI water to 10 % w/v solution. The solution was electrospun onto rotating mandrel with 5-cm diameter at rate of 5 ml/h and working distance of 10 cm. Total volume of 3 ml was electrospun with voltages +10 V and −3 V. The electrospun mats were cut into 3-mm wide strips and rolled into fibers that were used to create the hydrophilic core of the cortical scaffold.

Individual osteon-like scaffolds were electrospun onto rotating PEO fibers using a setup previously reported [36]. The fibers were loading into the setup and positioned in front of negatively charged target. The PLLA/gelatin mixture was electrospun first to a total volume of 1.5 ml, with the following parameters: working distance of 5 cm, at extrusion rate of 5 ml/h, and voltages of +17 V and −9 V. This was followed by electrospinning of PDLA solution (total volume of 0.5 ml) with the following parameters: working distance of 15 cm, extrusion rate of 5 ml/h, and voltages of +13 V and −8 V. All the scaffolds were crosslinked via vapor with 2.5 % glutaraldehyde for 2 h.

Heat Sintering of Scaffolds

The complete scaffolds were assembled by heat sintering individual components together at 54 °C for 45 min. The final

design consisted of 4 mm in diameter trabecular-like core surrounded by osteon-like segments and wrapped with a PDLA scaffold to a final diameter of 6 mm. This provided 2:1 ratio of trabecular to cortical section.

Dual layer PDLA and gelatin/PLLA mats were cut into 1.2-cm strips and rolled to 4-mm segments and heat sintered. Osteon-like scaffolds were cut into small segments and placed around the core, and everything was wrapped with electrospun sheet. The complete scaffolds were then heat sintered.

Mineralization of Scaffolds

All the scaffolds were mineralized using a previously reported method by incubation in 10× SBF [37, 38]. Briefly, a stock solution was made using NaCl, KCl, CaCl $2H_20$, $MgCl_2$ $6H_20$, and NaH_2PO_4, and stored at room temperature. Prior to the mineralization process, $NaHCO_3$ was added while stirring vigorously, resulting in the following ion concentrations: Ca^{2+} 25 mM, HPO_4^{2-} 10 mM, Na^+ 1.03 M, K^+ 5 mM, Mg^{2+} 5 mM, Cl^- 1.065 M, and HCO_3^- 10 mM. The electrospun cylindrical sintered 4 mm×12 mm scaffolds were incubated in 200 ml of 10× SBF for 6, 24, and 48 h at room temperature, with mineralizing solution replaced every 2 h. After being removed from 10× SBF, all the samples were rinsed in dI water to remove unattached mineral and vacuum-dried overnight.

Some of the scaffolds were pre-mineralized (Min0) by mineralizing individual osteons and electrospun sheets for 1 h, rinsed in dI water, and vacuum-dried overnight. The electrospun pieces were then heat sintered as described above.

Alizarin Red Staining

Mineral deposition and distribution was characterized using an Alizarin red stain. Alizarin red stain analysis is used to evaluate calcium deposition. The scaffolds were stained with 40-mM Alizarin red solution for 10 min. The scaffolds were then washed with dI water five times, placed into cryomolds, imbedded in OCT imbedding medium, and frozen at −20 °C. The scaffolds were cut into 200-μm section using a Cryostat HM 550 (Thermo Scientific Microm, Walldorf, Germany), and imaged using stereoscope (Vision Engineering, New Milford, CT, USA). Scaffolds from the cell study were fixed in 70 % ethanol for 1 h, rinsed in dI water, and the same protocol as above was followed.

Mechanical Properties

The scaffolds, n=6 per group, were mechanically tested in compression using an Instron 5869 with Bioplus Bath (Norwood, MA, USA). The tests were performed in phosphate buffered saline (PBS) (pH=7.4) at 37 °C. The groups were scaffolds mineralized for 6, 24, and 48 h. The 12 mm×6 mm (2:1 height to diameter ratio) scaffolds were tested in compression until failure with a uniform strain rate of 1.2 mm/min (10 % strain/min). The scaffolds satisfied the 2:1 aspect ratio requirement of the ASTM compression testing standard for rigid plastics (ASTM D695-02a). The data was analyzed to determine yield stress and compressive modulus.

Mineral Ash Weights

After the mechanical testing, the samples (n=3) were vacuum-dried overnight and used to determine mineral ash weights. After the initial weight of the samples was recorded, the samples were placed in ceramic crucibles, and then placed into a high temperature furnace (Model No. FD1535M, Fisher Scientific, Pittsburgh, PA, USA) at 700 °C for 24 h. After cooling down, the mineral ash weight was recorded and the average mineral percent deposition calculated as ratio of mineral ash weight to samples original weight.

In Vitro Study

Mouse pre-osteoblastic cells (MC3T3-E1, ATCC) were cultured in Alpha Minimum Essential Medium (α-MEM, Cellgro, Mediatech, Manassas, VA, USA) supplemented with 10 % fetal bovine serum (FBS, Cellgro, Mediatech, Manassas, VA, USA) and 1 % streptomycin/ penicillin (Cellgro, Mediatech, Manassas, VA, USA). The scaffolds were cut into 450-μm sections Cryostat HM 550 (Thermo Scientific Microm, Walldorf, Germany), soaked in di water overnight and vacuum-dried. The scaffolds were then secured into 24-well ultra-low cluster plates (Costar) using Silastic Medical Adhesive (Dow Corning, Midland, MI, USA) and were sterilized in 70 % ethanol for 30 min followed by exposure to UV light for 30 min. The scaffolds were then washed with PBS and soaked in cell culture medium overnight.

Two groups of scaffolds were used: scaffolds mineralized for 24 h (Min24) and non-mineralized (Min0) scaffolds. All the scaffolds were pre-mineralized as previously stated. Approximately, 100,000 cells were seeded onto each scaffold and were allowed to attach for 1 hour before adding culture medium to a final volume of 1 ml. Once the cells were attached, the media was supplemented with 3-mM β-glycerophospate and 10 μg/ml of L-ascorbic acid. The media was changed every other day, and the cultures were incubated at 37 °C in a humidified atmosphere and 5 % CO_2. Cells were cultured for a period of 28 days and data was collected on days 7, 14, 21, and 28.

Cell viability was measured using a Cell Titer 96^{TM} Aqueous Solution Cell Proliferation Assay (MTS Assay) (Promega, Madison, WI, USA) on the following scaffolds Min0 (n=6) and Min24 (n=6). At each time point (7, 14, 21, and 28 days), the media was removed, then 300 μl of fresh media and 60 μl

of the MTS solution were added to each well and incubated at 37 °C with 5 % CO_2 for 3 hours. After incubation, 300 μl of the mixture was transferred to a 48-well plate and diluted with 300 μl of DI water. The plate was read at 490 nm using a plate reader. Calibration curve with known cell numbers was performed on the beginning of the study to correlate MTS absorbance values to cell numbers.

Osteocalcin ELISA Assay

Osteocalcin (OCN) is a non-collagenous protein produced by mature osteoblasts during later stages of differentiation. It was measured in the media using an ELISA kit from Biomedical Technologies, Inc (Stoughton, MA). Media samples (n=4) were collected over the course of 28 days and stored at −80 °C until the end of study. The assay was performed according to the manufactures instructions and absorbance was read at 450 nm. Osteocalcin content is normalized to cell number and expressed as ng/cell.

Alizarin Red and Fluorescence Stain

We utilized the alizarin red stain assay to evaluate mineral deposition and distribution. At each time point, the scaffolds were washed with PBS and transferred into new well plates. The scaffolds were then fixed in 70 % ethanol for 1 h at 4 °C, and stained with 40 mM Alizarin red solution for 10 min. The scaffolds were then washed with DI water five times, placed into cryomolds, imbedded in OCT imbedding medium, and frozen at −20 °C. The scaffolds were cut into 50 μm section using a Cryostat HM 550 (Thermo Scientific Microm, Walldorf, Germany), and imaged using light microscope (Leica Microsystems LAS AF 6000, Bannockburn, IL, USA).

Statistical Analysis

Statistical analysis was performed using JMP 9 Software. All data was subjected to a one-way analysis of variance (ANOVA) with post-hoc analysis (Tukey test) to determine the statistical significance of differences between groups, $p<0.05$.

Results

In this study, we fabricated complete three-dimensional electrospun scaffolds and mineralized the scaffolds via static incubation in 10X SBF. The scaffolds were composed of dual structures, inner core surrounded by osteon-like scaffolds, shown in Fig. 1. The scaffolds were then further characterized to determine mechanical properties, mineral deposition and distribution, and cellular activity on the scaffolds.

Alizarin Red Staining

Mineral distribution across the scaffolds was observed using the alizarin red staining. Staining of the scaffolds was performed two ways to evaluate the calcium deposition throughout the scaffold and determine the optimal technique for this procedure. First, the scaffolds were stained with alizarin red and then sectioned and imaged, shown in Fig. 1 a–c, and then scaffolds were also sectioned and individual sections were stained and imaged, shown in Fig. 1 d–f. When the scaffolds were stained and then section (Fig. 1 a–c) mineral can be seen on the outer edges of the scaffolds with some mineral also found on inside of the osteons channels. No significant differences can be seen between mineralization times. When the scaffolds were sectioned then stained, much more mineral stain can be seen on the scaffolds. After 6 h of mineralization (Fig. 1 d), mineral can be seen on the outer edges and on the osteons, but absent from the central core. After 24 and 48 h (Fig. 1 e and f), scaffolds are completely covered in mineral, and no differences can be seen between two mineralization times.

Mineral Ash Weights

Mineral ash weights were determined to quantify the amount of mineral present on the scaffolds and are shown in Table 2. Increasing the mineralization time resulted in an increase mineral deposition, and each mineralization time point was significantly higher than the other two time points.

Mechanical Properties

Scaffolds were tested under simulated physiological conditions in compression at 10 % strain rate/min. Data was analyzed to determine yield stress and compressive modulus and is shown in Fig. 2. No significant differences in mechanical properties were seen between 0 and 6 h of mineralization or between 24 and 48 h of mineralization, but there was significant increase in yield stress at 24 and 48 h hours. Scaffolds mineralized for 24 and 48 h had significantly higher yield stresses than scaffolds mineralized for 6 and 0 h. Scaffolds mineralized for 24 h had significantly higher compressive modulus than non-mineralized scaffolds (0 h).

Cell Study

Proliferation of the M3T3-E1 cells on the scaffolds was quantified using an MTS assay at days 7, 14, 21, and 28. The absorbances at 490 nm are shown in Fig. 3. Over the course of 4 weeks, no differences were observed between the groups at any time point. Both groups did experience significant increase in absorbance over 28 days, Min0 group from day 7 to day 14 to day 21, and Min24 group from day 14 to day 28.

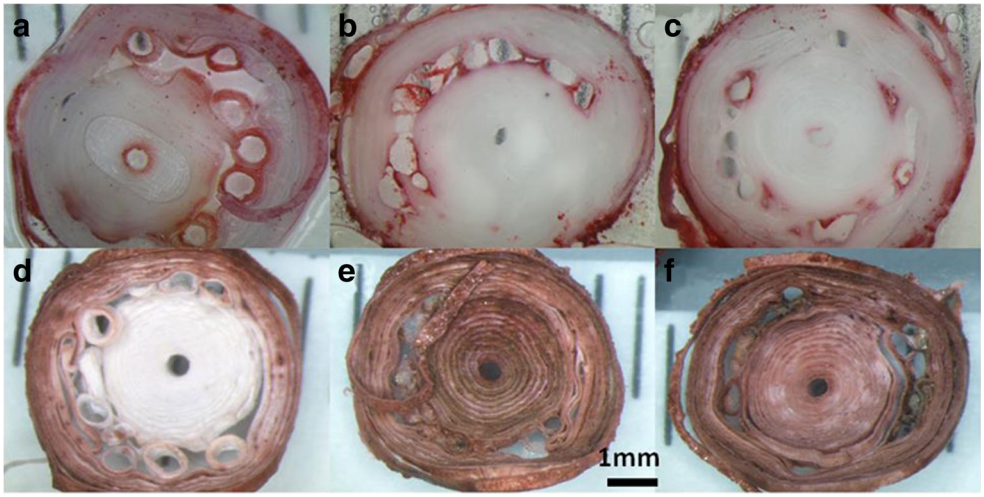

Fig. 1 *Top row*: Alizarin red staining images of scaffolds stained after (**a**) 6 h, (**b**) 24 h, (**c**) 48 h mineralization and then sectioned into 450 μm. *Bottom row*: Alizarin red staining images of scaffolds sectioned then stained after (**d**) 6 h, (**e**) 24 h, (**f**) 48 h mineralization

Osteocalcin ELISA Assay

Expression of osteocalcin, a primary bone marker, by the MC3T3-E1 pre-osteoblast cells was measured via ELISA over 28 days. The expression of osteocalcin indicates early stages of increased osteoblastic-like cellular behavior. Figure 4 shows the amount of OCN protein detected in the media as measured by the ELISA kit and normalized by cell number. There was an increase in OCN secretion during the last 2 weeks of the study. Also, there was significant increase in OCN secretion by the MC3T3-E1 cells seeded on the mineralized scaffolds during days 18–20 and 25–27.

Alizarin Red and Fluorescence Stain

At each time point during the cell study, the scaffolds were fixed and stained with alizarin red to visualize mineral deposition and distribution. The images are shown in Fig. 5. On day 0, prior to the start of the study, small amount of mineral can be seen on the Min0 scaffold from the premineralization treatment and a much greater amount of mineral can be seen on the Min24 scaffolds. Over the course of study increased amount of mineral can be seen with both scaffold groups, but overall, Min24 scaffolds seem to have more uniform mineral present.

Table 2 Mineral ash weight percentages. Mineral ash weight significantly increased (post-hoc ANOVA $p<0.5$) as mineralization time increases

Mineralization time (hr)	Mineral Ash Weight
6	6.33 %±0.91 %
24	17.01 %±2.99 %
48	26.18 %±0.85 %

Discussion

In this study, we fabricated complete three-dimensional electrospun scaffolds and mineralized them by incubation in 10× SBF. The scaffolds were composed of dual structures, inner core composed of wrapped electrospun sheets surrounded by osteon-like scaffolds which can be seen in Fig. 1. Few attempts have been made to create dual structure scaffolds that mimic natural bone organization. One includes biphasic foam scaffolds with varying degrees of porosities where the more dense scaffolds are found in the middle surrounded by an outer ring with higher degree of porosity. The scaffolds are made by heat sintering hydroxyapatite particles over porous polymeric sponges at very high temperatures [28, 34].

Figure 1 also shows the alizarin red stains of mineral on scaffolds that were stained before and after sectioning the scaffolds. When the scaffolds were stained before sectioning, some mineral can be seen on the edges and inside the channels, but overall, no major differences can be observed between mineralization times. When the scaffolds were sectioned and then stained, much more mineral can be seen especially on the 24- and 48-h mineralized scaffolds, which are completely covered. When we compared the amount of mineral found on the scaffolds, each mineralization time was significantly higher than the previous one.

Scaffolds were tested under simulated physiological conditions in compression at 10 % strain rate/min to determine mechanical properties. A significant increase in mechanical properties was observed after 24 h of mineralization both in compressive modulus and yield stress. The presence of mineral significantly increased the mechanical properties. While there was a qualitative difference in mineralization between the scaffolds mineralized for 24 and 48 h, the mechanical properties were not statistically significant. This is commonly seen with scaffolds that are mineralized by static incubation

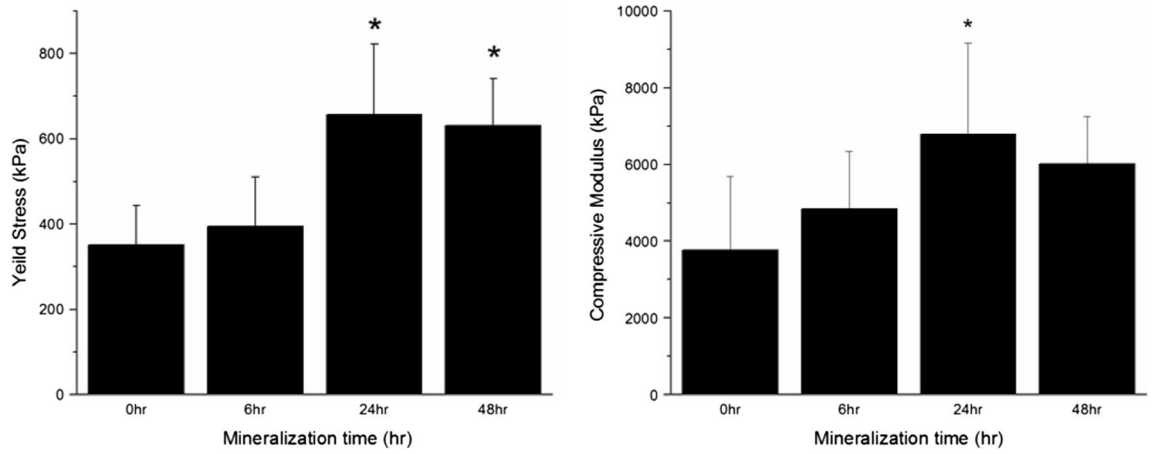

Fig. 2 Compressive yield stress (kPa) and compressive modulus (kPa) (10 % strain/min) of non-mineralized scaffolds and scaffolds mineralized for 6, 24, or 48 h. Statistical analysis: *denotes significance from 0 to 6 h mineralization for yield stress and 0 h mineralization for compressive modulus ANOVA Tukey Test (post-hoc) $p<0.05$

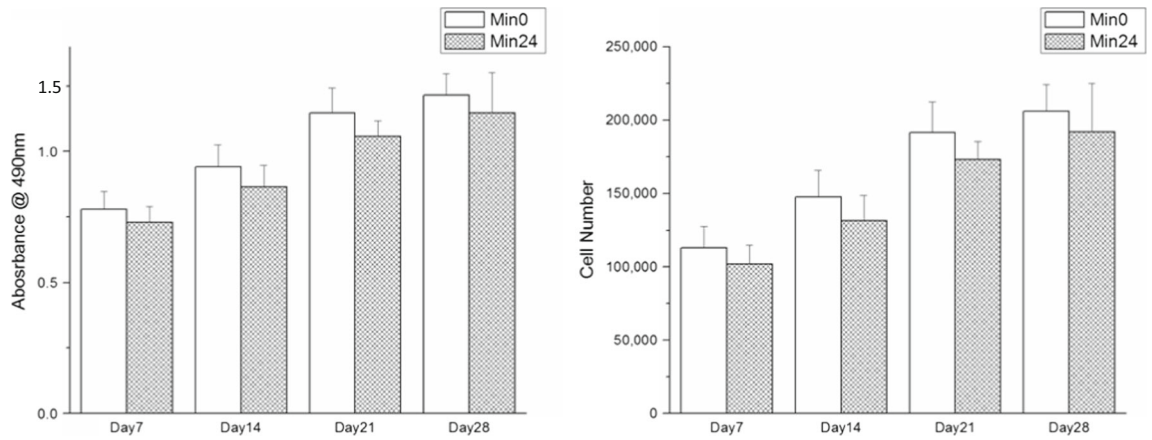

Fig. 3 MTS absorbance over the 4-week cell study (*left*) and cell numbers determined from MTS curve (*right*). MTS absorbance evaluated as the indirect measure of cellular viability. The highest absorbance exhibited at day 28 is 1.20

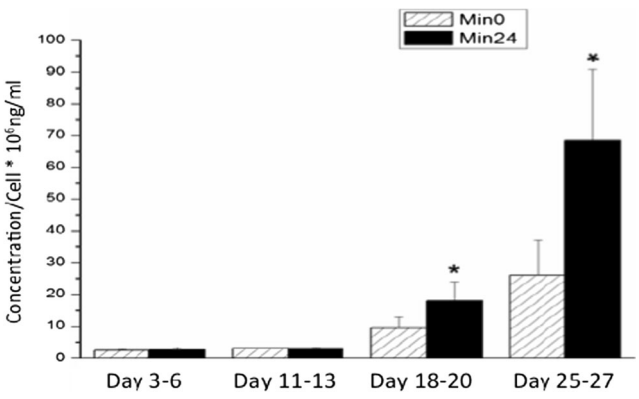

Fig. 4 Secreted OCN protein in cell culture media evaluated via ELISA. Results normalized to cell number determined by MTS assay. Statistical analysis: *denotes significance from Min0 by ANOVA Tukey Test (post-hoc) $p<0.05$

in SBF. Teo et al. utilized a flow chamber to mineralize electrospun scaffolds by alternately immersing them in $CaCl_2$ and Na_2HPO_4. This resulted in a more uniform deposition throughout the scaffold, and showed that mineral distribution is more important than overall mineral amount in the scaffolds [39]. The mechanical properties exhibited by the scaffolds were still lower than native bone properties. This could be attributed to the slight degradation of the material created during the mineralization study over the course of 28 days or the loosening of the polymer layers during mechanical testing. Current studies are being performed to decrease the amount of mineralized time needed for enhanced mineral deposition and creating more uniform tightly wrapped structures. Preliminary results conclude the scaffolds mineralized via electrodeposition for 6 h exhibited mechanical properties within the range of trabecular bone.

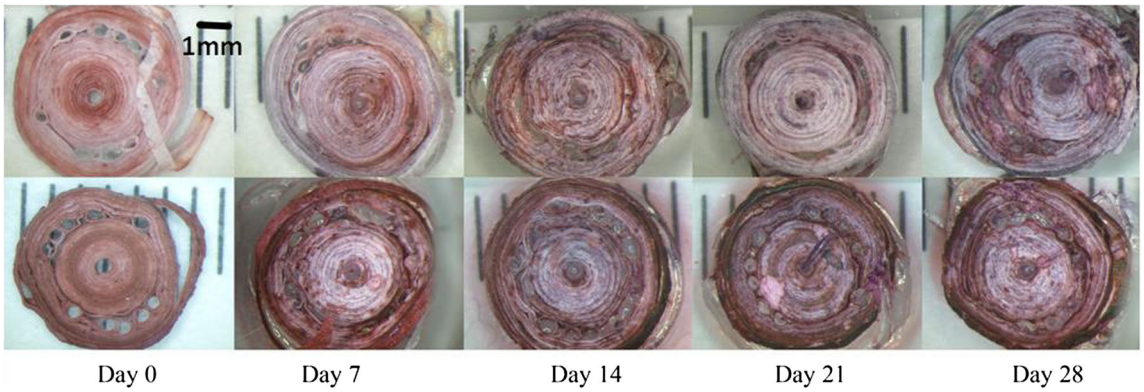

Fig. 5 Alizarin red stain pictures of 450-μm thick scaffold sections Min0 (*top*) and Min24 (*bottom*) over period of 28 days

Cellular attachment and proliferation were evaluated as mitochondrial activity as measured by the MTS assay over the period of 4 weeks. Over the course of the study, both groups of scaffolds supported proliferation of MC3T3-E1 cells, as significant increase in absorbance were observed. Based on the cell numbers as determined by MTS assay, the population of cells doubled after 28 days. However, no differences between mineralized and non-mineralized scaffolds were observed. Similar results were seen in previous work [36, 37] and work published by White et al. [40]. This can be explained by the competing processes of cellular proliferation and differentiation, where one decreases as the other increases [41]. Our results for the expression of OCN protein, shown in Fig. 4, further confirmed this. Scaffolds that have been mineralized show significantly higher levels of secreted OCN protein, a non-collagenous protein found in bone and expressed by differentiated osteoblasts. By the end of study, OCN expression on mineralized scaffolds was almost two-fold higher than non-mineralized scaffolds. This finding is consistent with previously reported results [40, 42].

At the end of each week, scaffolds were fixed and stained with alizarin red to visualize the mineral deposition on the scaffolds (Fig. 5). Over the course of the cell study, non-mineralized scaffolds became mineralized, especially around osteon channels. Mineralized scaffolds had much more mineral to start with, but over the course of the study displayed an increase in mineral in certain areas, namely edges and osteon channels. This shows that cells on site mineralized the matrix, which was previously observed in our work [36] and supported by other researchers [40].

Lack of cells on the center regions could be explained by the loss of microfiber morphologies due to cryostat sectioning of the scaffolds. As the cutting is performed at −20 °C, it can result in plastic deformation of fibers. Loss of microfiber morphology can be seen on SEM of cryostat sectioned scaffolds (Fig. 6). So, the insides of the osteon channels and outside edges could be the only regions there electrospun fiber morphology was preserved. However, we do not foresee this being a problem in the future, as these scaffolds were only sectioned for the purposes of this study.

Conclusion

In this study, we successfully fabricated a complete three-dimensional electrospun scaffold which mimics the highly packed osteonal structure of the native cortical bone and porous architecture of the native trabecular bone. Our dual structure scaffold was composed of an inner core of tightly wrapped electrospun sheets surrounded by osteon-like scaffolds. Scaffolds were successfully mineralized in 10× SBF up to 48 h and showed uniform mineral distribution throughout the scaffolds. Mineralization for 24 h significantly increased mechanical properties of the scaffolds in both yield stress and compressive modulus under physiological conditions, in comparison to the lower mineralization times. Both the non-mineralized and mineralized scaffold supported mouse pre-osteoblastic cellular attachment and proliferation over 28 days in vitro. Additionally, scaffolds mineralized for 24 h promoted osteoblastic

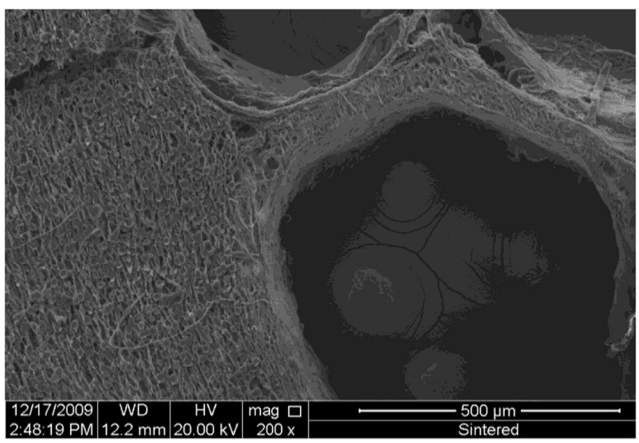

Fig. 6 SEM image of scaffolds sectioned using cryostat where fiber melting is visible on the surface

differentiation and mineral deposition. Based on the in vitro work presented, we expect the scaffold to perform efficiently in vivo with enhanced mechanics and cellular response due to the biochemical and mechanical influences from the surrounding microenvironment. Current ongoing work focuses on the development of an endothelial lumen within the cortical channel and simultaneous differentiation of human mesenchymal stem cells (hMSCs) along the osteoblastic and angiogeneic lineage for long-term graft mechanics and viability in vivo. Preliminary results conclude the ability of the tissue-engineered scaffold mentioned in this work to promote early stages of 2D angiogenic tube formation in vitro. The results of this study demonstrate the ability to fabricate a structural relevant tissue-engineered scaffold as an alternative to the current bone grafting treatments.

References

1. Hing KA. Bone repair in the twenty-first century: biology, chemistry or engineering? Philos Transact A Math Phys Eng Sci. 2004;362(1825):2821–50.
2. Giannoudis PV, Dinopoulos H, Tsiridis E. Bone substitutes: an update. Injury. 2005;36 Suppl 3:S20–7.
3. Research TM. Bone Grafts and Substitutes Market expected to reach USD 3.48 Billion Globally in 2023. Albany, NY. Bone Grafts and Substitutes Market - Global Industry Analysis, Size, Share, Growth, Trends and Forecast 2015–2023, 2015. <url: http://www.transparencymarketresearch.com/bone-grafts-substitutes-market.html>
4. Ritchie RO, *How does human bone resist fracture?* Ann N Y Acad Sci. 1192;1:72–80.
5. Rho JY, Kuhn-Spearing L, Zioupos P. Mechanical properties and the hierarchical structure of bone. Med Eng Phys. 1998;20(2):92–102.
6. Beniash E, *Biominerals-hierarchical nanocomposites: the example of bone.* Wiley Interdiscip Rev Nanomed Nanobiotechnol.
7. An YH, Draughn RA. Mechanical testing of bone and the bone-implant interface. Boca Raton: CRC Press; 2000. 624 p.
8. Cowin SC, Doty SB. Tissue mechanics. New York: Springer. xvi; 2007. 682 p.
9. Khan Y et al. Tissue engineering of bone: material and matrix considerations. J Bone Joint Surg Am. 2008;90 Suppl 1:36–42.
10. Liu X, Ma PX. Polymeric scaffolds for bone tissue engineering. Ann Biomed Eng. 2004;32(3):477–86.
11. Rezwan K et al. Biodegradable and bioactive porous polymer/inorganic composite scaffolds for bone tissue engineering. Biomaterials. 2006;27(18):3413–31.
12. Stevens B et al. A review of materials, fabrication methods, and strategies used to enhance bone regeneration in engineered bone tissues. J Biomed Mater Res B Appl Biomater. 2008;85(2):573–82.
13. Yang S et al. The design of scaffolds for use in tissue engineering. Part I Tradit Factors Tissue Eng. 2001;7(6):679–89.
14. Yu NY, et al. *Biodegradable poly(alpha-hydroxy acid) polymer scaffolds for bone tissue engineering.* J Biomed Mater Res B Appl Biomater. 93;1: 285–95.
15. Hutmacher DW et al. State of the art and future directions of scaffold-based bone engineering from a biomaterials perspective. J Tissue Eng Regen Med. 2007;1(4):245–60.
16. Karageorgiou V, Kaplan D. Porosity of 3D biomaterial scaffolds and osteogenesis. Biomaterials. 2005;26(27):5474–91.
17. Stylios G, Wan T, Giannoudis P. Present status and future potential of enhancing bone healing using nanotechnology. Injury. 2007;38 Suppl 1:S63–74.
18. Ma PX, Zhang R. Microtubular architecture of biodegradable polymer scaffolds. J Biomed Mater Res. 2001;56(4):469–77.
19. Maquet V et al. Porous poly(alpha-hydroxyacid)/Bioglass composite scaffolds for bone tissue engineering. I: Preparation and in vitro characterisation. Biomaterials. 2004;25(18):4185–94.
20. Chen VJ, Ma PX. Nano-fibrous poly(L-lactic acid) scaffolds with interconnected spherical macropores. Biomaterials. 2004;25(11):2065–73.
21. Liao CJ et al. Fabrication of porous biodegradable polymer scaffolds using a solvent merging/particulate leaching method. J Biomed Mater Res. 2002;59(4):676–81.
22. An YH, Woolf SK, Friedman RJ. Pre-clinical in vivo evaluation of orthopaedic bioabsorbable devices. Biomaterials. 2000;21(24):2635–52.
23. Lu L et al. In vitro and in vivo degradation of porous poly(DL-lactic-co-glycolic acid) foams. Biomaterials. 2000;21(18):1837–45.
24. Borden M et al. Tissue engineered microsphere-based matrices for bone repair: design and evaluation. Biomaterials. 2002;23(2):551–9.
25. Borden M et al. Structural and human cellular assessment of a novel microsphere-based tissue engineered scaffold for bone repair. Biomaterials. 2003;24(4):597–609.
26. Lv Q, Nair L, Laurencin CT. Fabrication, characterization, and in vitro evaluation of poly(lactic acid glycolic acid)/nano-hydroxyapatite composite microsphere-based scaffolds for bone tissue engineering in rotating bioreactors. J Biomed Mater Res A. 2009;91(3):679–91.
27. Shah AR et al. Migration of Co-cultured Endothelial Cells and Osteoblasts in Composite Hydroxyapatite/Polylactic Acid Scaffolds. Ann Biomed Eng. 2011;39(10):2501–9.
28. Son JS et al. Hydroxyapatite/polylactide biphasic combination scaffold loaded with dexamethasone for bone regeneration. J Biomed Mater Res. 2011;99A(4):638–47.
29. Laurencin CT, Nair LS. Biodegradable polymers as biomaterials. Prog Polym Sci. 2007;32(8–9):762–98.
30. Middleton JC, Tipton AJ. Synthetic biodegradable polymers as orthopedic devices. Biomaterials. 2000;21(23):2335–46.
31. Wang H et al. Biocompatibility and osteogenesis of biomimetic nano-hydroxyapatite/polyamide composite scaffolds for bone tissue engineering. Biomaterials. 2007;28(22):3338–48.
32. Hak DJ. The use of osteoconductive bone graft substitutes in orthopaedic trauma. J Am Acad Orthop Surg. 2007;15(9):525–36.
33. Gazdag AR et al. Alternatives to Autogenous Bone Graft: Efficacy and Indications. J Am Acad Orthop Surg. 1995;3(1):1–8.
34. Jang JH, Castano O, Kim HW. Electrospun materials as potential platforms for bone tissue engineering. Adv Drug Deliv Rev. 2009;61(12):1065–83.
35. Liao S et al. Processing nanoengineered scaffolds through electrospinning and mineralization suitable for biomimetic bone tissue engineering. J Mech Behav Biomed Mater. 2008;1(3):252–60.
36. Andric T, Sampson AC, Freeman JW. Fabrication and characterization of electrospun osteon mimicking scaffolds for bone tissue engineering. Mater Sci Eng C-Mater Biol Appl. 2011;31(1):2–8.
37. Andric T, Wright LD, Freeman JW. *Rapid Mineralization of Electrospun Scaffolds for Bone Tissue Engineering.* J Biomater Sci Polym Ed.

38. Tas AC, Bhaduri SB. Rapid coating of Ti6A14V at room temperature with a calcium phosphate solution similar to 10x simulated body fluid. J Mater Res. 2004;19(9):2742–9.
39. Teo WE, et al. *Fabrication and characterization of hierarchically organized nanoparticle-reinforced nanofibrous composite scaffolds.* Acta Biomater. 7;1: 193–202.
40. Whited BM et al. Pre-osteoblast infiltration and differentiation in highly porous apatite-coated PLLA electrospun scaffolds. Biomaterials. 2011;32(9):2294–304.
41. Owen TA et al. Progressive development of the rat osteoblast phenotype in vitro: reciprocal relationships in expression of genes associated with osteoblast proliferation and differentiation during formation of the bone extracellular matrix. J Cell Physiol. 1990;143(3):420–30.
42. Chou YF, Dunn JC, Wu BM. In vitro response of MC3T3-E1 pre-osteoblasts within three-dimensional apatite-coated PLGA scaffolds. J Biomed Mater Res B Appl Biomater. 2005;75(1):81–90.